

## DEGRADATION OF MALACHITE GREEN USING GREEN SYNTHESIZED IRON NANOPARTICLES BY *Coffea arabica* LEAF EXTRACTS AND ITS ANTIBACTERIAL ACTIVITY

Gaminda K A P<sup>1</sup> Thomas I B K<sup>1</sup> Lakmayuri P<sup>1</sup> Abeyasinghe D T<sup>1</sup> Jayasinghe C D<sup>2</sup> Senthilnithy R<sup>1</sup>

Department of Chemistry, The Open University of Sri Lanka, Nugegoda, Sri Lanka<sup>1</sup>


Department of Zoology, The Open University of Sri Lanka, Nugegoda, Sri Lanka<sup>2</sup>

### ABSTRACT

The synthesis of biocompatible nanomaterials using bio-renewable plant extract has emerged as a promising alternative to traditional methods in recent years due to its cost-effectiveness, eco-friendliness, non-toxicity, and biocompatibility. In this research paper, we demonstrate using *Coffea arabica* leaf extract to synthesize zero-valent iron nanoparticles (GC-FeNPs). This study suggests that this method is efficient and environmentally friendly, making it a promising approach for developing biocompatible nanomaterials. The synthesized GC-FeNPs were characterized using Fourier-Transform Infrared (FT-IR), X-ray diffraction (XRD), scanning electron microscope (SEM), and UV-Vis spectroscopy techniques. According to the analysis of data, polyphenolic/caffeine compounds in the coffee leaf extract act as reducing/capping agents by converting the  $Fe^{2+}$  to  $Fe^0$ , and minimizing the aggregation. The FT-IR and XRD data confirm the encapsulation of the GC-FeNPs by the polyphenolic/caffeine compounds in the coffee leaf extract. The GC-FeNPs have a quasi-spherical shape morphology with a particle size of about 80 – 100 nm. Further, dye degrading ability, and the antibacterial activity of the GC-FeNPs were investigated using malachite green (MG) and gram-negative and gram-positive pathogens. Experimental data revealed that GC-FeNPs ( $\sim 20 \pm 1$  mg) showed degradation activity against MG up to 55 % upon the 120-minute incubation. Furthermore, the kinetic analysis of GC-FeNPs on MG degradation was in accordance with the pseudo-second-order kinetic model ( $R^2 = 0.9922$ ). In addition, GC-FeNPs showed an antibacterial activity against gram-negative (*E. coli*, and *S. enterica*), and gram-positive (*S. aureus*) pathogens. The *E. coli* growth was highly inhibited by the GC-FeNPs compared to other strains. Overall, GC-FeNPs facilitate an alternative approach to degrade MG from textile effluents and industrial wastewater and treat the pathogen-contaminated water.

**KEYWORDS:** Green synthesis, Iron nanoparticles, *C. arabica*, Malachite green, Degradation, Antibacterial activity

Corresponding Author: Abeyasinghe D. T., Email: dtabe@ou.ac.lk

 <https://orcid.org/0000-0003-2454-5104>



This is an open-access article licensed under a Creative Commons Attribution 4.0 International License (CC BY) allowing distribution and reproduction in any medium crediting the original author and source.

## 1. INTRODUCTION

Water is an essential element on the earth, and numerous living organisms rely on it. However, water quality is degrading consistently due to various contaminations. Dyes play a significant role in water contamination all over the world. Annually, 700,000 tons of synthetic dyes are used worldwide for the dyeing operation process; around 15 -20 % end up in wastewater and find their way to the environment (Basturk and Karatas, 2015). Dye is a very harmful compound to the environment and living organisms due to its reactivity (Leme *et al.*, 2015; Xiao *et al.*, 2020). Aquatic plants are highly affected due to dye contamination in water since dye colour promotes turbidity (Khandare and Govindwar, 2015; Verma and Samanta, 2018). Turbidity in water bodies reduces the penetration of the sun's rays into the water body and affects photosynthesis.

Further, the biotransformation of the dyes into different products poses various threats to living organisms and the environment. However, due to the photo and heat stability, most dyes do not degrade quickly in the environment (Basturk and Karatas, 2015). Therefore, for the past few decades, novel techniques have been developed to treat wastewater contaminated by dyes. Also, degradation by techniques such as physicochemical adsorption (Gao, Si and He, 2015), electrocoagulation (Kobyia *et al.*, 2014), membrane filtration (Chidambaram, Oren and Noel, 2015), nano-filtration (Paździor *et al.*, 2009), ozonation (Panda and Mathews, 2014), Fenton oxidation, and oxidation processes were identified as good strategies (Soares *et al.*, 2015). However, the formation of toxic compounds may reduce the effectiveness of these methods. Therefore, biodegradation of the dye has been employed using aerobic and anaerobic bacteria (Popli and Patel, 2015), Sequencing Batch Reactor (SBR) (Santos and Boaventura, 2015), *etc.* These biological processes were further found to be effective to a certain extent but challenging to sustain in dye-contaminated wastewater.

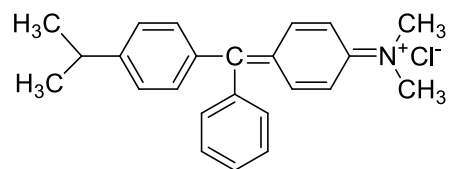


**Figure 1: Chemical structure of the malachite green**

Malachite green (MG) is a cationic triphenylmethane (Figure 1) dye used in the dyeing process in different industries such as fabrics, paint, inks, leather, *etc.* (Huang *et al.*, 2014a; Xiao *et al.*, 2020). It is vital to remove MG from wastewater before discharging into the environment due to its toxicity. Therefore, different methods such as the adsorption (Gao, Si and He, 2015), biological degradation (Tsai, and Chen, 2010; Yatome *et al.*, 1993), and photocatalytic degradation (Wu *et al.*, 1999; Hachem *et al.*, 2001; Elango and Roopan, 2015), are employed to remove MG content in the wastewater. However, due to the drawbacks such as high cost and low efficiency associated with these techniques, the applicability in the degradation process of MG is limited to a certain extent. Therefore, novel remediation techniques as an alternative are required to remove MG in wastewater effectively.

Recently, nano zero-valent iron (nZVI) has attracted research interest in groundwater treatment due to the higher intrinsic reactivity of its surface sites (Iravani, 2011; Dutta *et al.*, 2016). Numerous chemical and physical approaches have been deployed for the synthesis of nZVI. However, these physical methods are associated with drawbacks such as energy consumption, expensiveness, the requirement of sophisticated laboratories, *etc.* (Sun *et al.*, 2006; Nadagouda *et al.*, 2010; Huang *et al.*, 2014b). Sodium borohydride (NaBH<sub>4</sub>) is commonly used as a reducing agent in the chemical synthesis of nZVI (Devatha, Thalla and Katte, 2016). However, reducing agents such as NaBH<sub>4</sub>, stabilizing agents, capping agents, and organic solvents in chemical synthesis are limited due to the expense and toxic effect on the environment (Sun *et al.*, 2006;

Nadagouda *et al.*, 2010; Huang *et al.*, 2014b). The green synthesis of nZVI has been identified as an alternative approach due to its cost-effectiveness, eco-friendliness, biodegradability, and non-toxicity. Green synthesis received much attention due to the usage of bio-renewable natural sources (Tandon, Shukla and Singh, 2013; Huang *et al.*, 2014a; Wang, Fang and Megharaj, 2014; Das and Eun, 2018). Recently, various nanomaterials have been synthesized using different green extracts (Njagi *et al.*, 2011; Mohan Kumar *et al.*, 2013; Zhu *et al.*, 2018). Generally, components such as polyphenols available in tea and coffee extract have emerged as an alternative for the chemical synthesis of nZVI since they can act as both a reducing and capping agent (Mohan Kumar *et al.*, 2013; Ouyang *et al.*, 2019). This feature of the green extract reduces the aggregation and the oxidation of the nZVI particles (Chen *et al.*, 2011). The green synthesis of nZVI using green extract polyphenols has been investigated for biocompatibility, degrading bromothymol blue by the Fenton oxidation process (Shahwan *et al.*, 2011), and degradation of the trichloroethylene (TCE) by developing Fe/Pd membrane using a green tea extract (Smuleac *et al.*, 2011). Fenton-like catalytic properties of the green synthesized iron nanoparticles (FeNPs) have been investigated for the degradation of dyes. The reactivity of the green synthesized FeNPs is significantly dependent on the reducing and capping agents of the green extract. Various green extracts promote different reactivities of the green synthesized FeNPs, (Raveendran, Fu and Wallen, 2003; Makarov *et al.*, 2014). The FeNPs synthesized using green extracts have been employed for dye adsorption and eutrophication remediation (Lin *et al.*, 2017).

Researchers have recently used tea extracts to synthesize iron nanoparticles for the selective removal of MG from wastewater. (Huang *et al.*, 2014a, 2014b; Xiao *et al.*, 2020). In 2014, Huang's group (Huang *et al.*, 2014a) conducted a similar study utilizing FeNPs synthesized using tea extracts. The results indicated that the removal efficiency of MG was 81.6%, with an equilibrium

at around 60 minutes. The rate kinetics were better fitted to the pseudo-first-order model ( $R^2 = 0.925$ ). The experiment was conducted using 0.01 g/L of nanomaterial, which was incubated with an 8 mL 50-ppm solution of MG. A recent study by Xiao's group (Xiao *et al.*, 2020) reported that FeNPs synthesized using green methods could effectively remove MG from wastewater. The researchers reported a degradation efficiency of 95.14% for MG, with an equilibrium achieved at approximately 100 minutes. The rate kinetics of the process were found to be better described by the pseudo-first-order model, with an  $R^2$  value of 0.95. The study was conducted by utilizing 0.01 g of nanomaterial incubated in a 50-ppm solution of MG. The observed deviations in batch experiment analysis may be attributed to the variations in experimental conditions and the quantity and composition of polyphenolic compounds used for encapsulating iron nanomaterials. The specific experimental conditions, such as temperature, pressure, and pH level, as well as the type and concentration of polyphenolic compounds in the plant extracts used for the synthesis process, could impact the physicochemical properties of the iron nanoparticles. These physicochemical properties, in turn, may influence the behaviour and performance of the nanoparticles in the batch experiment analysis, resulting in deviations. This study aims to synthesize FeNPs from *Coffea arabica* leaf extract and characterize the FeNPs using SEM, FT-IR, UV-Vis, and XRD analysis. The reactivity of FeNPs in malachite green degradation and antibacterial activity against gram-positive and gram-negative bacteria were also evaluated. To the best of our knowledge, this is the first study that reports on the antibacterial and degradation effect of malachite green in the presence of green synthesized FeNPs using *Coffea arabica* leaf extract.

## **2. METHODOLOGY**

### **A. Materials**

Ferrous sulfate heptahydrate (99%,  $\text{FeSO}_4 \cdot 7\text{H}_2\text{O}$ ) was purchased from Sigma Aldrich, and malachite green (MG) was purchased from DYECHEM

(Colombo, Sri Lanka). *Coffea arabica* (coffee) leaves were collected from local farms. Muller Hinton Agar from Hi-Media Laboratories and deionized (DI) water was used in all experiments.

## B. Preparation of leaf extract

Fresh coffee leaves were collected from a local farm and washed thoroughly with DI water to clean the leaf's surface. Leaves were dried at room temperature. Twenty-five grams of dry leaves of *C. arabica* were cut into small pieces and mixed with 150.0 mL of deionized water (Figure 2). The temperature of the solution was maintained at 60 °C and kept on stirring for 1 hour. The resulting solution was allowed to cool to room temperature and filtered using gravity filtration. The green extract was stored at -4 °C for further use.

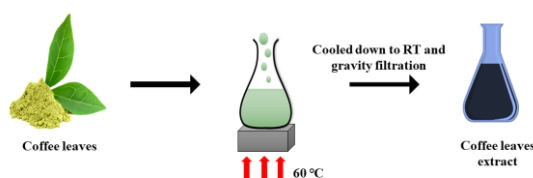


Figure 2: Preparation of the coffee extract

## C. Green synthesis of iron particles

Coffee FeNPs (GC-FeNPs) were synthesized, as shown in Figure 3. The coffee leaf extract was added to 0.10 M  $\text{FeSO}_4$  solution with a volume ratio of 1:1 at room temperature and continuously stirred at 75 °C for 1 hr. The immediate colour change to black colour indicated the formation of GC-FeNPs. As synthesized GC-FeNPs were separated using gravity filtration. The product was washed three times with ethanol to remove the remaining residues of the coffee leaf extract and dried using a vacuum oven at 25 °C for 24 hrs.

## D. Characterization

The synthesized nanomaterials were characterized using UV-Vis, FT-IR, SEM, and XRD techniques.

### 1. UV-Vis spectroscopy

The absorption spectra of GC-FeNPs treated solutions were analyzed using UV-Visible

spectrophotometer (ChromTech, CT-2600, Taiwan).

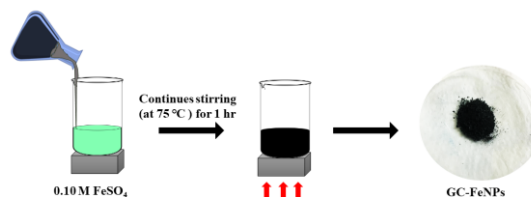


Figure 3: Preparation of the GC-FeNPs

### 2. Fourier transform infrared spectroscopy (FT-IR)

Fourier Transform Infrared Spectroscopy (FT-IR) analysis of GC-FeNPs was done over the range of 4000 - 400  $\text{cm}^{-1}$  to investigate the fabrication of GC-FeNPs by the coffee leaf extract. The measurements were performed on a FT-IR spectrometer (Bruker Vertex80 FT-IR spectrometer, Germany).

### 3. Scanning electron microscopy (SEM)

The microstructure and size of the GC-FeNPs were characterized using scanning electron microscopy (Carl Zeiss Evo 18 Research, Germany). SEM images of the sample were obtained at different magnifications using an operating voltage of 20 kV.

### 4. X-ray diffraction (XRD)

The crystallinity state of GC-FeNPs was analyzed by X-ray diffraction (Rigaku SmartLab X-Ray Powder Diffractometer, Japan) using with Cu-K $\beta$  radiation source at room temperature. It was operated at 40Kv/30mA over  $2\theta$  range of 5 to 80°. The scanning speed was maintained at 10  $\text{min}^{-1}$ .

## E. Degradation of malachite green – Batch experiment

The removal efficiency of MG was evaluated using GC-FeNPs; 100  $\mu\text{L}$  suspension of GC-FeNPs was ( $\sim 20 \pm 1$  mg) added to a solution containing 100 ppm MG (25.0 mL). Then, the conical flasks were placed in a rotary shaker at 298 K and 150 r/min. After a decided specific time, the degraded solutions were taken out and filtered through Whatman No. one filter paper to remove the GC-FeNPs. The resulting solution was

analyzed to determine the remaining concentration of MG. A calibration plot of absorbance vs concentration for the MG was prepared using a standard series to evaluate the MG concentration of the degraded solution. According to the UV-Vis spectroscopy the maximum wavelength ( $\lambda_{max}$ ) for the MG was identified as 617 nm. Hence, the absorbance of the degraded MG solution was measured using a UV-Spectrophotometer at 617 nm. The removal efficiency ( $\eta$ ) and the amount of absorbed dye per unit mass of sorbent at a given time ( $q_t$ , mg/g) and equilibrium ( $q_e$ , mg/g) using GC-FeNPs were calculated by using the following equations (Wang and Li, 2013; Katata-Seru *et al.*, 2018; Gao *et al.*, 2019):

$$\eta = \frac{C_0 - C_t}{C_0} \times 100 \% \quad (1)$$

$$q_t = (C_0 - C_t)V/W \quad (2)$$

$$q_e = (C_0 - C_e)V/W \quad (3)$$

Where  $\eta$  = the MG removal efficiency,  $C_0$  = the initial MG concentration in the solution (ppm),  $C_t$  = the MG concentration at a time (ppm), and  $C_e$  = the MG concentration at the equilibrium (ppm). All experiments were undertaken in triplicate, and the error values are not very significant.

#### F. Antibacterial activity studies

The antibacterial activities of green synthesized GC-FeNPs and antibiotic compound streptomycin were evaluated against gram-negative *Escherichia coli* (*E. coli* ATCC 25922), *Salmonella enterica* ATCC 14028, and gram-positive *Staphylococcus aureus* ATCC 25923 by disk diffusion method using Muller Hinton agar (MHA) medium (Prakash *et al.*, 2013; Elango and Roopan, 2015). Briefly, microbes were grown on nutrient agar at 37 °C for 24 hrs. Afterward, fresh nutrient agar was inoculated with the overnight culture and incubated until the optical density at 600 nm ( $OD_{600}$ ) reached 0.5. Then, the bacterial suspensions were spread on the MHA plates using a sterile spreader. Sterile Whatman No. one paper discs at 6 mm dimension were impregnated with coffee leaf extract and GC-FeNPs. The disc with

streptomycin antibiotic compound was used as the positive control reference. These discs were gently pressed in MHA plates and incubated in an inverted position at 37 °C for 24 hrs to determine the Zone of inhibition. All experiments were undertaken in duplicate.

### 3. RESULTS AND DISCUSSION

#### A. FT-IR analysis

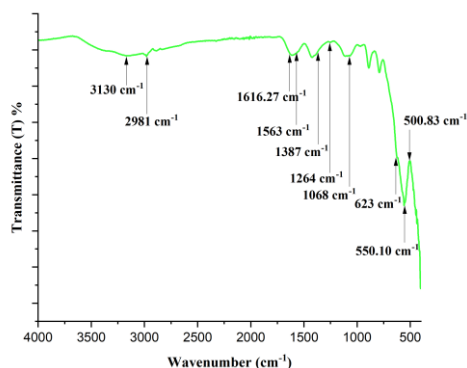
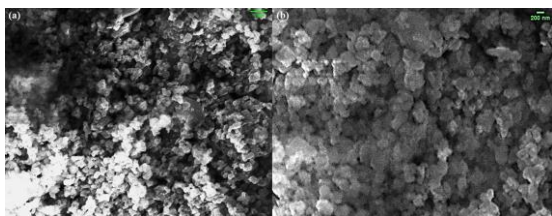


Figure 4: FT-IR spectra of the GC-FeNPs

The FT-IR analysis identified different functional groups in the synthesized GC-FeNPs (Figure 4). FT-IR spectra showed eight significant peaks in the 400-1700  $cm^{-1}$  range. Several studies have reported that different functional groups were responsible for green GC-FeNPs synthesis (Shahwan *et al.*, 2011; Akhbari *et al.*, 2019). According to the FT-IR spectra, stretching vibrational bands at 2981  $cm^{-1}$ , 1068  $cm^{-1}$ , and 3129.54  $cm^{-1}$ , correspond to stretching vibrations of C-H, C-O-C, and OH bonds (Lopez *et al.*, 2010; Wang *et al.*, 2014; T. *et al.*, 2020; Xiao *et al.*, 2020; Parthipan *et al.*, 2021). The peaks at 1616  $cm^{-1}$  and 1387  $cm^{-1}$  attribute for C-N of aromatic amines (Lopez *et al.*, 2010; Wang *et al.*, 2014; T. *et al.*, 2020; Xiao *et al.*, 2020; Parthipan *et al.*, 2021). The absorption band at 1563  $cm^{-1}$  is related to the conjugated system of benzene (Lopez *et al.*, 2010; Wang *et al.*, 2014; T. *et al.*, 2020; Xiao *et al.*, 2020; Parthipan *et al.*, 2021), which confirms the functionalization of the GC-FeNPs by the polyphenols/caffeine compounds in the coffee leaf extract. Furthermore, peaks at 550.10  $cm^{-1}$  and 500.83  $cm^{-1}$  correspond to the Fe-O vibrational

stretches, which confirms the formation FeNPs using coffee extract as a reducing and capping agent (Lopez *et al.*, 2010; Wang *et al.*, 2014; T. *et al.*, 2020; Xiao *et al.*, 2020; Parthipan *et al.*, 2021).

### B. SEM analysis



**Figure 5: SEM images of the GC-FeNPs (a) 15 KX and (b) 25 KX magnification**

The morphologies and size of GC-FeNPs were determined by SEM, as shown in Figure 5, which indicated the successful synthesis of iron nanoparticles. SEM images of GC-FeNPs revealed that the morphology of the iron particles is in quasi-spherical shaped nanoparticles with a diameter ranging from 80 - 100 nm (Smuleac *et al.*, 2011). Further, many GC-FeNPs form irregular clusters consistent with the previously reported green synthesized iron-based nanoparticles (Njagi *et al.*, 2011; Shahwan *et al.*, 2011). The size distribution of the GC-FeNPs mainly occurs due to the reducing properties associated with natural compounds in the coffee green extract. Also, these compounds act as a capping agent and a stabilizer to avoid the oxidation of the zero-valent iron particles ( $\alpha$ -Fe<sup>0</sup>) when exposed to the air. (Wang *et al.*, 2014)

### C. XRD analysis

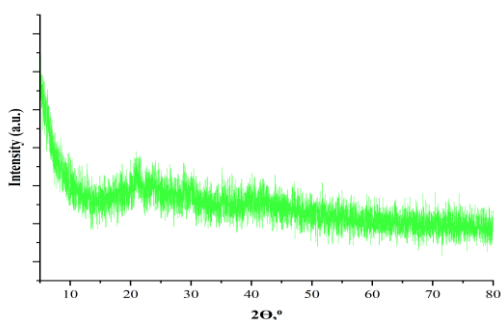


**Figure 6: XRD pattern of the GC-FeNPs**

The X-ray diffractometer analysis was explored to identify the crystalline nature of the synthesized GC-FeNPs (Figure 6). The XRD pattern shows that the GC-FeNPs are an amorphous structure. The  $\alpha$ -Fe<sup>0</sup> surface has been encapsulated by coffee leaf extract polyphenols/caffeine, which function as a dispersive and capping agent in the synthesis process, as confirmed by the FT-IR analysis of the GC-FeNPs. The broad shoulder peak at 21.43° is determined to be the absorption peak of polyphenols/caffeine in the coffee extract (Njagi *et al.*, 2011; Cao *et al.*, 2016). The broad peak around 45° on the G<sub>n</sub>ZVI corresponds to the  $\alpha$ -Fe<sup>0</sup> (Huang *et al.*, 2014a; Wang *et al.*, 2014; Dutta *et al.*, 2016; Katata-Seru *et al.*, 2018; Xiao *et al.*, 2020).

### D. Degradation of malachite green and kinetic studies

#### 1. Degradation of Malachite Green (MG)

Figure 7(a) illustrates the degradation of the MG using the GC-FeNPs at different periods. The characteristic absorption peak of MG, which is attributed to the -C=C- functional group, is located at 617 nm. (Wang *et al.*, 2017; Xiao *et al.*, 2020) As decolorization occurs, the peak at 617 nm decreases with time due to the reactivity of GC-FeNPs. This signifies the remarkable potential of GC-FeNPs in degrading MG from the aqueous system by cleaving the -C=C- bond of the MG. (Wang *et al.*, 2017; Xiao *et al.*, 2020) According to Figure 7 (a), the initial concentration of the MG 100 ppm was reduced to 64.9 ppm after 20 min of incubation with the GC-FeNPs. Then, the MG concentration gradually decreased, and the MG concentration at equilibrium was 45 ppm. According to Figure 7(b), degradation efficiency reached 51 % at 40 min, and degradation efficiency reached 55 % at 120 min. These data indicate valuable insights for the development of more effective and sustainable methods for the removal of MG from aqueous systems.

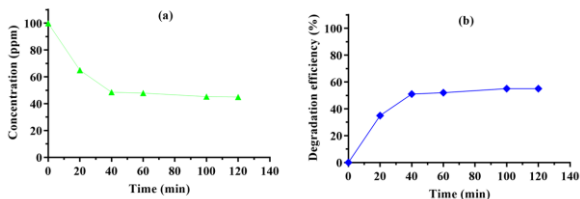


**Figure 7: (a) Variation of the MG concentration with time upon the GC-FeNPs incubation, (b) MG degradation efficiency with time upon the GC-FeNPs incubation**

## 2. Kinetic Studies

The adsorption kinetics of the MG onto adsorbent (GC-FeNPs) were investigated using pseudo-first-order and pseudo-second-order equations. These models are highly dependent on adsorbent material's physical and chemical characteristics. The pseudo-first-order is more suitable for lower concentrations of the solution, and the pseudo-first-order rate equation can be expressed as follows (Wang *et al.*, 2014; Gao *et al.*, 2019):

$$\ln(q_e - q_t) = \ln q_e - k_1 t \quad (4)$$

Where  $q_e$  and  $q_t$  (mg/g) are the amounts of MG molecules adsorbed on the GC-FeNPs at equilibrium and at different times  $t$  ( $\text{min}^{-1}$ ) and  $k_1$  is the rate constant of the pseudo-first-order model for the adsorption process ( $\text{min}^{-1}$ ). The linear plot of  $\ln(q_e - q_t)$  against time, as shown in Figure 8(a), was used to calculate the rate constant  $k_1$ . The slope of the linear plot gives the value for the  $k_1$ .

The pseudo-second-order kinetic model equation is expressed as follows (Bhattacharyya and Gupta, 2008; Gao *et al.*, 2019):

$$\frac{dq_t}{dt} = k_2 (q_e - q_t)^2 \quad (5)$$

Integrating Eq. (5) by applying the boundary conditions  $t = 0$  to  $t$  and  $q_t = 0$  to  $t$ , gives:

$$\frac{1}{(q_e - q_t)} = \frac{1}{q_e} + k t \quad (6)$$

When Eq. (6) linearized, it expressed as follows:

$$\frac{t}{q_t} = \frac{1}{k_2 q_e^2} + \left(\frac{1}{q_e}\right) t \quad (7)$$

Where,  $q_e$  and  $q_t$  (mg/g) are the amounts of MG molecules adsorbed on the GC-FeNPs at equilibrium and at different times  $t$  ( $\text{min}^{-1}$ ) and  $k_2$  ( $\text{g mg}^{-1} \text{min}^{-1}$ ) is the rate constant of the pseudo-second-order model for the adsorption process. Values of the  $k_2$  and  $q_e$  can be determined from the plot of  $t/q_t$  against  $t$ , as shown in Figure 8(b).

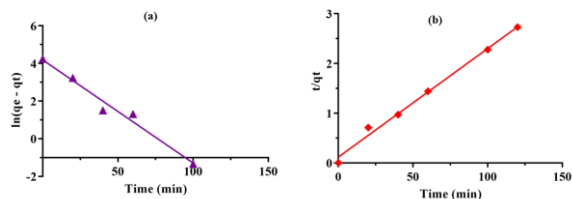


**Figure 8: (a) Pseudo-first-order kinetics of GC-FeNPs and (b) pseudo-second-order kinetics of the GC-FeNPs**

**Table 1. The kinetic parameters of MG degradation by GC-FeNPs**

Dye type	Pseudo First Order		Pseudo Second Order	
	$K_1$ ( $\text{min}^{-1}$ )	$R_1^2$	$K_2$ ( $\text{g mg}^{-1} \text{min}^{-1}$ )	$R_2^2$
MG (100 ppm)	0.0548	0.9760	0.0040	0.9922

The correlation coefficients ( $R^2$ ) show that MG adsorption onto the GC-FeNPs was better fitted for the pseudo-second-order ( $R^2 = 0.9922$ ) compared to the pseudo-first-order model, according to Table 1. Therefore, the adsorption of MG onto GC-FeNPs did not follow the pseudo-first-order model but well-fitted the pseudo-second-order model.

## E. Antibacterial activity

The antibacterial activity of the GC-FeNPs was evaluated using the gram-negative *Escherichia coli* (*E. coli* ATCC 25922), *Salmonella enterica* ATCC 14028, and gram-positive *Staphylococcus aureus* ATCC 25923 by disk diffusion assay (Figure 9).

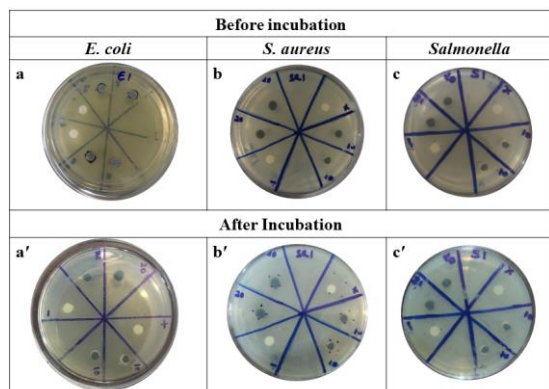


**Figure 9: Zone of inhibition (a) *E. coli*, (b) *S. aureus* and (c) *Salmonella***

The inhibitory activity of the synthesized GC-FeNPs (10  $\mu\text{L}$  and 20  $\mu\text{L}$ ) with varying concentrations against the tested isolates was tested. The Pathogens' Zone of inhibition (DIZ)

values ranged from 0.6 to 1.1 cm, as indicated in Figure 9. This study used various control groups such as coffee leaf extract, positive control (streptomycin), and distilled water, to inhibit pathogens.

**Table 2. Zone of inhibition obtain in antibacterial activity**

Concentration ( $\mu\text{L}$ )	<i>E. coli</i> (cm)	<i>S. aureus</i> (cm)	<i>Salmonella</i> (cm)
10	$0.9 \pm 0.1$	$0.9 \pm 0.0$	$0.6 \pm 0.0$
20	$1.1 \pm 0.1$	$1.0 \pm 0.0$	$0.8 \pm 0.0$

According to the study, GC-FeNPs exhibited a predominant role against pathogenic bacteria such as *E. coli* (10  $\mu\text{L}$  – 0.9 cm, 20  $\mu\text{L}$  – 1.1 cm) and *S. aureus* (10  $\mu\text{L}$  – 0.9 cm, 20  $\mu\text{L}$  – 1.0 cm) compared to the *Salmonella* (10  $\mu\text{L}$  – 0.6 cm, 20  $\mu\text{L}$  – 0.8 cm) as shown in Table 2. The positive nature of GC-FeNPs could promote antibacterial activity due to the interactions with the cellular membrane of gram-negative and gram-positive pathogens by disrupting the cell membrane and producing reactive oxygen species (Hu *et al.*, 2019; Sadek, Asker and Abdelhamid, 2021).

However, the coffee leaf extract shows no antibacterial activity against the bacterial strains selected in this study.

#### 4. CONCLUSION

In this study, the green synthesis of FeNPs was carried out with *Coffea arabica* leaf extract, and FT-IR, XRD, and SEM analysis confirmed the formation of GC-FeNPs. The polyphenols/caffeine in the coffee leaf extract acted as a reducing and capping agent that reduced the aggregation of the GC-FeNPs. The FT-IR analysis confirms the functionalization of GC-FeNPs by the polyphenolic/caffeine compounds in the coffee leaf extract. Also, XRD data confirm the availability of  $\alpha\text{-Fe}^0$  and encapsulation of GC-FeNPs by the polyphenolic/caffeine. At the same time, the SEM analysis shows that the synthesized GC-FeNPs have a quasi-spherical shape morphology with a particle size of about 80 – 100 nm. The green synthesized GC-FeNPs can be utilized in environmental applications such as the toxic dye MG degradation process. The experimental data confirmed that the GC-FeNPs could effectively degrade the 100 ppm MG in an aqueous solution by using a 100  $\mu\text{L}$  suspension ( $\sim 20 \pm 1$  mg) of GC-FeNPs compared to the previously reported MG degradation using nanomaterials synthesized using different plant extracts. The MG degradation efficiency by GC-FeNPs reached 45 ppm (55 % degradation efficiency) with an equilibrium around 120 minutes. The kinetic study of the MG degradation revealed that the degradation of MG by GC-FeNPs is well-fitted with the pseudo-second-order adsorption model ( $R^2 = 0.9922$ ). In addition, the GC-FeNPs showed potential antibacterial activity against *E. coli* and *S. aureus* compared to *Salmonella*. The antibacterial activity of the GC-FeNPs increased with higher concentration, and the growth of *E. coli* strain was highly inhibited by the GC-FeNPs. Therefore, GC-FeNPs can be explored as a promising nanomaterial for treating contaminated water sources, particularly for removing toxic dyes.



## ACKNOWLEDGEMENTS

This work was supported by the Accelerating Higher Education Expansion and Development (AHEAD) operation in Sri Lanka. Development oriented Research grant 28., The Open University of Sri Lanka.

## 5. REFERENCES

- Akhbari, M. *et al.* (2019). 'Process optimisation for green synthesis of zerovalent iron nanoparticles using *Mentha piperita*', *IET Nanobiotechnology*, 13(2), pp. 160–169.
- Basturk, E. and Karatas, M. (2015). 'Decolorization of antraquinone dye Reactive Blue 181 solution by UV/H<sub>2</sub>O<sub>2</sub> process', *J. of Photochemistry and Photobiology A: Chemistry*, 299, pp. 67–72.
- Bhattacharyya, K.G. and Gupta, S. Sen (2008). 'Adsorption of a few heavy metals on natural and modified kaolinite and montmorillonite: A review', *Advances in Colloid and Interface Science*, pp. 114–131.
- Cao, D. *et al.* (2016). 'Removal of phosphate using iron oxide nanoparticles synthesized by eucalyptus leaf extract in the presence of CTAB surfactant', *Chemosphere*, 159, pp. 23–31.
- Chen, Z.X. *et al.* (2011) 'Removal of methyl orange from aqueous solution using bentonite-supported nanoscale zerovalent iron', *J. of Colloid and Interface Science*, 363(2), pp. 601–607.
- Chidambaram, T., Oren, Y. and Noel, M. (2015). 'Fouling of nanofiltration membranes by dyes during brine recovery from textile dye bath wastewater', *Chemical Engineering J.*, 262, pp. 156–168.
- Das, P.R. and Eun, J.B. (2018). 'A comparative study of ultra-sonication and agitation extraction techniques on bioactive metabolites of green tea extract', *Food Chemistry*, 253, pp. 22–29.
- Devatha, C.P., Thalla, A.K. and Katte, SY (2016) 'Green synthesis of iron nanoparticles using different leaf extracts for treatment of domestic waste water', *J. of Cleaner Production*, 139, pp. 1425–1435.
- Dutta, S. *et al.* (2016) 'Rapid reductive degradation of azo and anthraquinone dyes by nanoscale zerovalent iron', *Environmental Technology and Innovation*, 5, pp. 176–187.
- Elango, G. and Roopan, S.M. (2015). 'Green synthesis, spectroscopic investigation and photocatalytic activity of lead nanoparticles', *Spectrochimica Acta - Part A: Molecular and Biomolecular Spectroscopy*, 139, pp. 367–373.
- Gao, J., Si, C. and He, Y. (2015). 'Application of soybean residue (okara) as a low-cost adsorbent for reactive dye removal from aqueous solution', *Desalination and Water Treatment*, 53(8), pp. 2266–2277.
- Gao, S. *et al.* (2019). 'Adsorption of anionic dye onto magnetic Fe<sub>3</sub>O<sub>4</sub>/CeO<sub>2</sub> nanocomposite: Equilibrium, kinetics, and thermodynamics', *Adsorption Science and Technology*, 37(3–4), pp. 185–204.
- Hachem, C. *et al.* (2001). 'Decolourization of textile industry wastewater by the photocatalytic degradation process', *Dyes and Pigments*, 49(2), pp. 117–125.
- Hu, Y. *et al.* (2019). 'Roles of extracellular polymeric substances in the bactericidal effect of nanoscale zerovalent iron: trade-offs between physical disruption and oxidative damage', *Environmental Science: Nano*, 6(7), pp. 2061–2073.
- Huang, L. *et al.* (2014). 'Green synthesis of iron nanoparticles by various tea extracts: Comparative study of the reactivity', *Spectrochimica Acta - Part A: Molecular and Biomolecular Spectroscopy*, 130, pp. 295–301.
- Huang, L. *et al.* (2014). 'Synthesis of iron-based nanoparticles using oolong tea extract for the degradation of malachite green', *Spectrochimica Acta - Part A: Molecular and Biomolecular Spectroscopy*, 117, pp. 801–804.
- Iravani, S. (2011). 'Green synthesis of metal nanoparticles using plants', *Green Chemistry*, 13(10), pp. 2638–2650.
- Katata-Seru, L. *et al.* (2018). 'Green synthesis of iron nanoparticles using *Moringa oleifera* extracts and their applications: Removal of nitrate from water and antibacterial activity against *Escherichia coli*', *J. of Molecular Liquids*, 256, pp. 296–304.
- Khandare, R.V. and Govindwar, S.P. (2015). 'Phytoremediation of textile dyes and effluents: Current scenario and future prospects', *Biotechnology Advances*. Elsevier, pp. 1697–1714.
- Kobyas, M. *et al.* (2014). 'Treatment of textile dyeing wastewater by electrocoagulation using Fe and Al electrodes: Optimisation of operating parameters using central composite design', *Coloration Technology*, 130(3), pp. 226–235.

- Leme, DM *et al.* (2015). 'Eco- and genotoxicological assessments of two reactive textile dyes', *J. of Toxicology and Environmental Health - Part A: Current Issues*, 78(5), pp. 287–300.
- Lin, J. *et al.* (2017). 'Characterization and reactivity of iron based nanoparticles synthesized by tea extracts under various atmospheres', *Chemosphere*, 169, pp. 413–417.
- Lopez, J.A. *et al.* (2010). 'Synthesis and characterization of Fe<sub>3</sub>O<sub>4</sub> magnetic nanofluid', *Revista Latinoamericana de Metalurgia y Materiales*, 30(60), pp. 60–66.
- Makarov, V. V. *et al.* (2014). 'Biosynthesis of stable iron oxide nanoparticles in aqueous extracts of hordeum vulgare and rumex acetosa plants', *Langmuir*, 30(20), pp. 5982–5988.
- Mohan Kumar, K. *et al.* (2013). 'Biobased green method to synthesise palladium and iron nanoparticles using Terminalia chebula aqueous extract', *Spectrochimica Acta - Part A: Molecular and Biomolecular Spectroscopy*, 102, pp. 128–133.
- Nadagouda, M.N. *et al.* (2010). 'In vitro biocompatibility of nanoscale zerovalent iron particles (NZVI) synthesized using tea polyphenols', *Green Chemistry*, 12(1), pp. 114–12.
- Njagi, E.C. *et al.* (2011). 'Biosynthesis of iron and silver nanoparticles at room temperature using aqueous sorghum bran extracts', *Langmuir*, 27(1), pp. 264–271.
- Ouyang, Q. *et al.* (2019). 'Green synthesis of Fe-based material using tea polyphenols and its application as a heterogeneous Fenton-like catalyst for the degradation of lincomycin', *J. of Cleaner Production*, 232, pp. 1492–1498.
- Panda, K.K. and Mathews, A.P. (2014). 'Ozone oxidation kinetics of Reactive Blue 19 anthraquinone dye in a tubular in situ ozone generator and reactor: Modeling and sensitivity analyses', *Chemical Engineering J.*, 255, pp. 553–567.
- Parthipan, P. *et al.* (2021). 'Evaluation of Syzygium aromaticum aqueous extract as an eco-friendly inhibitor for microbiologically influenced corrosion of carbon steel in oil reservoir environment', *Bioprocess and Biosystems Engineering*, 44(7), pp. 1441–1452.
- Paździor, K. *et al.* (2009). 'Integration of nanofiltration and biological degradation of textile wastewater containing azo dye', *Chemosphere*, 75(2), pp. 250–255.
- Popli, S. and Patel, U.D. (2015). 'Destruction of azo dyes by anaerobic–aerobic sequential biological treatment: a review', *Int. J. of Environmental Science and Technology*. Center for Environmental and Energy Research and Studies, pp. 405–420.
- Prakash, P. *et al.* (2013). 'Green synthesis of silver nanoparticles from leaf extract of Mimosa pudica for enhanced antibacterial activity against multi drug resistant clinical isolates', *Colloids and Surfaces B: Biointerfaces*, 108, pp. 255–259.
- Raveendran, P., Fu, J. and Wallen, S.L. (2003) 'Completely "Green" Synthesis and Stabilization of Metal Nanoparticles', *J. of the American Chemical Society*, 125(46), pp. 13940–13941.
- Sadek, A.H., Asker, M.S. and Abdelhamid, S.A. (2021). 'Bacteriostatic impact of nanoscale zerovalent iron against pathogenic bacteria in the municipal wastewater', *Biologia*, 76(9), pp. 2785–2809.
- Santos, S.C.R. and Boaventura, R.A.R. (2015). 'Treatment of a simulated textile wastewater in a sequencing batch reactor (SBR) with addition of a low-cost adsorbent', *J. of Hazardous Materials*, 291, pp. 74–82.
- Shahwan, T. *et al.* (2011). 'Green synthesis of iron nanoparticles and their application as a Fenton-like catalyst for the degradation of aqueous cationic and anionic dyes', *Chemical Engineering J.*, 172(1), pp. 258–266.
- Smuleac, V. *et al.* (2011). 'Green synthesis of Fe and Fe/Pd bimetallic nanoparticles in membranes for reductive degradation of chlorinated organics', *J. of Membrane Science*, 379(1–2), pp. 131–137.
- Soares, P.A. *et al.* (2015). 'Enhancement of a solar photo-Fenton reaction with ferric-organic ligands for the treatment of acrylic-textile dyeing wastewater', *J. of Environmental Management*, 152, pp. 120–131. A
- Sun, Y.P. *et al.* (2006). 'Characterization of zerovalent iron nanoparticles', *Advances in Colloid and Interface Science*, pp. 47–56.
- T., S.J.K. *et al.* (2020). 'Biosynthesis of multiphase iron nanoparticles using Syzygium aromaticum and their magnetic properties', *Colloids and Surfaces A: Physicochemical and Engineering Aspects*, 603, p. 125241.
- Tandon, P.K., Shukla, R.C. and Singh, S.B. (2013). 'Removal of arsenic(III) from water with clay-supported zerovalent iron nanoparticles synthesized with the help of tea liquor', *Industrial and*

*Engineering Chemistry Research*, 52(30), pp. 10052–10058.

Tsai, W. T., & Chen, H. R. (2010). Removal of malachite green from aqueous solution using low-cost chlorella-based biomass. *J. of hazardous materials*, 175(1-3), 844–849.

Verma, P. and Samanta, S.K. (2018). 'Microwave-enhanced advanced oxidation processes for the degradation of dyes in water', *Environmental Chemistry Letters*. Springer, pp. 969–1007.

Wang, L. and Li, J. (2013) 'Removal of methylene blue from aqueous solution by adsorption onto crofton weed stalk', *BioResources*, 8(2), pp. 2521–2536.

Wang, T. *et al.* (2014). 'Green synthesized iron nanoparticles by green tea and eucalyptus leaves extracts used for removal of nitrate in aqueous solution', *J. of Cleaner Production*, 83, pp. 413–419.

Wang, X. *et al.* (2017) 'Facile green synthesis of functional nanoscale zerovalent iron and studies of its activity toward ultrasound-enhanced decolorization of cationic dyes', *Chemosphere*, 166, pp. 80–88.

Wang, Z., Fang, C. and Megharaj, M. (2014). 'Characterization of iron-polyphenol nanoparticles synthesized by three plant extracts and their fenton oxidation of azo dye', *ACS Sustainable Chemistry and Engineering*, 2(4), pp. 1022–1025.

Wu, K. *et al.* (1999). 'Photo-Fenton degradation of a dye under visible light irradiation', *J. of Molecular Catalysis A: Chemical*, 144(1), pp. 77–84.

Xiao, C. *et al.* (2020). 'Green synthesis of iron nanoparticle by tea extract (polyphenols) and its selective removal of cationic dyes', *J. of Environmental Management*, 275(August), p. 111262.

Yatome, C. *et al.* (1993). 'Degradation of Crystal violet by *Nocardia corallina*', *Applied Microbiology and Biotechnology*, 38(4), pp. 565–569.

Zhu, F. *et al.* (2018). 'Green synthesis of nano zerovalent iron/Cu by green tea to remove hexavalent chromium from groundwater', *J. of Cleaner Production*, 174, pp. 184–190.